Mineralogical Magazine (2023), **87**, 396–406
doi:10.1180/mgm.2022.139

CAMBRIDGE UNIVERSITY PRESS

Article

Crystal structures of rhodium-containing erlichmanite–laurite solid solutions ($Os_{1-x-y}Ru_xRh_yS_2$: $x = 0.09–0.60$, $y = 0.07–0.10$) with unique compositional dependence

Ginga Kitahara[1]*, Akira Yoshiasa[1], Satoko Ishimaru[1], Kunihisa Terai[1], Makoto Tokuda[2], Daisuke Nishio-Hamane[3], Takahiro Tanaka[4] and Kazumasa Sugiyama[2]

[1]Graduate School of Science and Technology, Kumamoto University, Kumamoto 860-8555, Japan; [2]Institute for Materials Research, Tohoku University, Sendai 980-8577, Japan; [3]Institute for Solid State Physics, the University of Tokyo, Kashiwa, Chiba 277-8581, Japan; and [4]Sunagawa-cho, Tachikawa, Tokyo 190-0031, Japan

Abstract

Rh-rich and Ir-poor erlichmanite–laurite OsS_2–RuS_2 solid solutions have been discovered at placers in Haraigawa, Misato-machi, Kumamoto, Japan. Microprobe analysis was performed to identify solid solutions containing few sub-components other than Rh. Approximately 10 at.% Rh was found to be present in the solid-solution samples. Structural refinement was performed using four natural samples: $Os_{0.32}Ru_{0.61}Rh_{0.07}S_2$, $Os_{0.49}Ru_{0.43}Rh_{0.08}S_2$, $Os_{0.58}Ru_{0.33}Rh_{0.08}S_2$ and $Os_{0.81}Ru_{0.09}Rh_{0.10}S_2$. The unit-cell parameters for the solid solutions containing Rh from Haraigawa varied from 5.61826(6) to 5.63142(8) Å. The (Os, Ru, Rh)–S distances in the $Os_{1-x-y}Ru_xRh_yS_2$ system were almost constant with a small variation of 0.001 Å. Conversely, the S–S distances varied significantly, with variations approaching 0.1 Å. Rh substitution of Os rather than Ru had a larger impact on the crystal structure. The atomic displacement ellipsoid of both cations and anions was almost spherical, and no elongation along the *M*–S and S–S bond directions was observed. The bulk Debye temperatures were estimated from the Debye–Waller factor for the sulfide site. The bulk Debye temperatures of pure OsS_2 and RuS_2 were 688 K and 661 K, respectively, which suggests that the melting point of erlichmanite is higher than that of laurite. The high Debye temperature of OsS_2 is inconsistent with the crystallisation of laurite prior to erlichmanite from the primitive magma, which suggests that f_{S_2}, rather than temperature, is the main cause of the known crystallisation order. The presence of several percent Rh has a significant effect on the thermal stability of OsS_2 and lowers the melting point of the erlichmanite solid solution compared to that of the laurite solid solution.

Keywords: $Os_{1-x-y}Ru_xRh_yS_2$, laurite, erlichmanite, crystal structure, Debye temperature

(Received 25 May 2022; accepted 10 December 2022; Accepted Manuscript published online: 22 December 2022; Associate Editor: František Laufek)

Introduction

Laurite (RuS_2)–erlichmanite (OsS_2) solid-solution series

Laurite (ideal end-member: RuS_2) has long been known as a rare mineral and was described by Wöhler (1866). Conversely, erlichmanite (OsS_2) was discovered much more recently: erlichmanite present in a Pt–Fe alloy from placer deposits was first reported by Snetsinger (1971), and several other studies (Sutarno *et al.*, 1967; Leonard *et al.*, 1969; Harris, 1974; Begizov *et al.* 1976; Cabri, 2002) have detailed mineralogical descriptions of the laurite–erlichmanite solid-solution series compositions obtained from placer deposits. A complete solid solution can be formed between laurite and erlichmanite, with considerable substitution of Os and Ru by Ir, Rh, Pd and Pt (Leonard *et al.*, 1969; Snetsinger, 1971; Harris, 1974; Begizov *et al.*, 1976; Bowles *et al.*, 1983; Cabri, 2002). In most cases, laurite and erlichmanite contain elements in the order Ir, Rh, Pd and Pt, though Ni and Fe have been detected as trace elements (Cabri, 2002). Bowles *et al.* (1983) reported a very high Ir content of 0.04–0.13 atoms per formula unit (apfu) in some laurite–erlichmanite solid solutions. In solid solutions with Ru >0.15 apfu [$x > 0.15$ in $Os_{1-x-y}Ru_x(Ir,Rh,Pd,Pt)_yS_2$)], Ir is predominant over Rh. Thus, for the majority of the laurite–erlichmanite solid solutions, Ir is the predominant additional metal, causing a large fluctuation in the Ir/Rh atomic ratio. However, owing to significant amounts of transition metals such as Ir, Rh, Pd and Pt dissolved in naturally occurring laurite–erlichmanite solid-solution minerals (Bowles *et al.*, 1983), no systematic study of the structure of this solid solution has been conducted.

Members of the laurite–erlichmanite solid-solution series are common platinum-group minerals (PGM) in podiform chromite ores hosted by mantle peridotites in ophiolite complexes. They occur mainly as small mineral inclusions in chromites associated with other PGM, base-metal sulfides, and silicates (Stockman and Hlava, 1984; Legendre and Augé, 1986; Augé and Johan, 1988; Corrivaux and Gilles Laflamme, 1990; Torres-Ruiz *et al.*, 1996;

*Author for correspondence: Ginga Kitahara, Email: galaxy.kitahara@gmail.com
Cite this article: Kitahara G., Yoshiasa A., Ishimaru S., Terai K., Tokuda M. Nishio-Hamane D., Tanaka T. and Sugiyama K. (2023) Crystal structures of rhodium-containing erlichmanite–laurite solid solutions ($Os_{1-x-y}Ru_xRh_yS_2$: $x = 0.09–0.60$, $y = 0.07–0.10$) with unique compositional dependence. *Mineralogical Magazine* **87**, 396–406. https://doi.org/10.1180/mgm.2022.139

Melcher *et al.*, 1997; Garuti *et al.*, 1999a, 1999b; Ahmed and Arai, 2003; Gervilla *et al.*, 2005; González-Jiménez *et al.*, 2007; Arai, 2012). Several studies have reported that some laurite–erlichmanite crystals form directly from sulfur-undersaturated mafic melts prior to, or along with, the crystallisation of chromite, and that they act as nuclei for chromite crystallisation (Stockman and Hlava, 1984; Augé, 1985; Ahmed and Arai, 2003). The laurite–erlichmanite solid solution in depleted ophiolites are usually Ir rich and somewhat Rh poor. Laurite–erlichmanite solid solutions from different types of chromitite have certain characteristics in terms of the amount of trace elements in their solid solutions.

Two different types of placers are known for PGM, one corresponding to the iridium-subgroup element (IPGE: Ru, Os and Ir) distribution, and the other to the palladium-subgroup element (PPGE: Rh, Pd and Pt) distribution (Mertie, 1969; Ohta and Nakagawa, 1990; Harris and Cabri, 1991; Nakagawa and Ohta, 1993; Arai *et al.*, 1999). A bimodal distribution characterised by IPGE-rich and PPGE-rich chromitites is also known for the compositional tendency of the platinum-group elements. IPGE-rich chromitites are formed in the deeper mantle and PPGE-rich chromitites in the uppermost part of the mantle, near the Moho transition zone (Ferrario and Garuti, 1990; Leblanc, 1991; Garuti *et al.*, 1995; 1999a, 1999b; Ahmed and Arai, 2003). PGM from the depleted ophiolites tend to be rich in IPGE whereas PPGE-rich PGM originate from the host rock by partial melting of the upper mantle. PPGE tend to concentrate in magma because of their incompatible behaviour with IPGE (Matsumoto, 1928; Leblanc, 1991; Nakagawa *et al.*, 1991; Ahmed and Arai, 2003; Arai, 2012).

Platinum-group elements have a siderophile nature (Goldschmit, 1937), and tend to be strongly fractionated into sulfide phases. They are potentially useful indicators of the degree of partial melting in the mantle and the partial pressure of sulfur saturation in the melt (e.g. Arculus and Delano, 1981; Arai *et al.*, 1999). Because the composition of a laurite–erlichmanite solid-solution series should be influenced strongly by temperature and sulfur fugacity, f_{S_2} (Brenan and Andrews, 2001; Andrews and Brenan, 2002; Bockrath *et al.*, 2004), each individual inclusion may record valuable information on the thermodynamic conditions prevailing during its crystallisation (Augé and Johan, 1988; Nakagawa and Franco, 1997; Garuti *et al.*, 1999a). Detailed mineralogical investigations into the physical properties and structures of PGM solid solutions are required, in addition to petrological observations to understand this system.

Crystal structure of laurite (RuS_2) and erlichmanite (OsS_2)

Laurite and erlichmanite have the same pyrite-type structures. Both covalent and ionic bonds have been identified in pyrite-type compounds, and both high- and low-spin states have been observed in transition-metal pyrite-type compounds under ambient conditions (Elliot, 1960; Folmer *et al.*, 1988; Tokuda *et al.*, 2019). Many stable platinum-group chalcogenides have a pyrite-type structure (Furuseth *et al.*, 1965; Sutarno *et al.*, 1967; Stassen and Heyding, 1968), in addition Ru and Os belong to the same family as Fe in the periodic table. Pyrite (FeS_2) is a diamagnetic semiconductor in which Fe ions exist in a low-spin divalent state (Elliot, 1960; Folmer *et al.*, 1988); cattierite (CoS_2) has a pyrite-type structure (Nowack *et al.*, 1991); the existence of pyrite-type RhS_2 is unconfirmed, though data have been proposed for the unit-cell parameter of hypothetical RhS_2 (Thomassen, 1929; Hulliger, 1964); and pyrite-type IrS_2 has been synthesised under high pressures (Munson, 1968). Rhodium, a homologous element of Co and Ir, can have various valences and low- or high-spin states. The second and third transition metal cations in the complexes are usually in a low-spin state.

Lutz *et al.* (1990) and Stingl *et al.* (1992) refined the structures of synthetic RuS_2 and OsS_2 end-members, respectively, using single-crystal diffraction experiments. There are few detailed studies on the variation of crystal structure with composition in the laurite–erlichmanite system. In natural specimens, substitutions of various additional elements such as Ir, Rh, Pd and Pt occur simultaneously; therefore, no systematic study of the structure of the solid solution has been conducted.

Minerals with Rh-rich and Ir-poor laurite–erlichmanite solid-solution series compositions have recently been discovered as inclusions of isoferroplatinum (Pt_3Fe) from a mantle-derived ultramafic massif in PPGE-type placers in Kumamoto, Japan (Nishio-Hamane *et al.*, 2019). Erlichmanite and laurite are the most abundant inclusions in isoferroplatinum (Pt_3Fe), they form a wide range of solid solutions between Os and Ru, and a certain amount of Rh is also substituted in most cases. The solid-solution samples from this area form suitable crystals for investigating the effect of only Rh on the RuS_2–OsS_2 crystal structures.

Debye–Waller factors can be used for determining the quantitative changes in the vibration characteristics of materials. The Debye temperature Θ_D for each atom at a crystallographically independent site can be estimated using the dynamic component of the Debye–Waller factor based on the Debye approximation (Willis and Pryor, 1975; Wood *et al.*, 2002; Yoshiasa *et al.*, 2016; Yoshiasa *et al.*, 2021). The Debye temperatures are related to the mechanical and thermal properties of the materials; hence the Debye temperature is one of the physical quantities that can be compared for materials with different compositions. Occurrences such as the crystallisation order of mantle minerals can be discussed based on the Debye temperature.

Herein, the crystal structures of the pyrite-type $Os_{1-x-y}Ru_xRh_yS_2$ solid solutions ($x = 0.09$–0.60 and $y = 0.07$–0.10) were refined using natural samples from Haraigawa, Misato-machi, Kumamoto, Japan. We found a unique compositional dependence of the unit-cell parameters and S–S distances in the pyrite-type solid solution. When Os (not Ru) is replaced by Rh, an interesting phenomenon occurs in the solid-solution crystals. The substitution of Os by Rh in erlichmanite (OsS_2) has a significant effect on cell size, bonding distances and vibrational properties. This seems to be controlled by the structural requirements. Under structurally restricted environments in solid solutions, the electronic state of Rh as a subcomponent in solid solutions is different from that of the end-member pure crystal.

One of the aims of this study is to elucidate the nature of the unique chemical bonding state observed in the pyrite-type structure. Even in the well-known pyrite-type platinum-group element compounds, there are many unsolved themes in terms of chemical bonding state and ionic radii. Another aim is to clarify the mineralogical significance of accessory minerals and the important roles of minor elements on crystals. Unique and diverse effects of minor and subcomponent ions on the structural and physical properties have been observed in the Rh-bearing erlichmanite–laurite solid-solution system.

https://doi.org/10.1180/mgm.2022.139 Published online by Cambridge University Press

Experiments

Specimens and chemical analyses

The compositional characteristics of PGM found in a small stream crossing the clinopyroxenite mass at Haraigawa, Kumamoto, Japan (32°34' 15"N, 130°47'25"E) were consistent with those of the PPGE-rich placer (Nishio-Hamane *et al.*, 2019). The placer specimens were collected by panning the river sand from Haraigawa. Almost all grains were predominantly isoferroplatinum with diverse PPGE-based PGM. The grain size was generally <1 mm and rarely exceeded 2 mm. The PPGE-rich PGM in this region has been reported to be derived from the host rock owing to the partial melting of the upper mantle (Nishio-Hamane *et al.*, 2019). Ultramafic rocks are exposed along the Kurosegawa belt in central Kyushu, and clinopyroxenite, in association with serpentinite, is distributed in the Tomochi area of Kumamoto (Kanmera, 1952; Saito *et al.*, 2004, 2005). Clinopyroxenite is regarded as a cumulate that developed at the bottom of the magma chamber and is generated by partial melting of the upper mantle. Osanai *et al.* (2014) considered that clinopyroxenite in the serpentine mélange of the Kurosegawa belt was formed by the accumulation of crystals at the base of a magma chamber under the mid-ocean ridge.

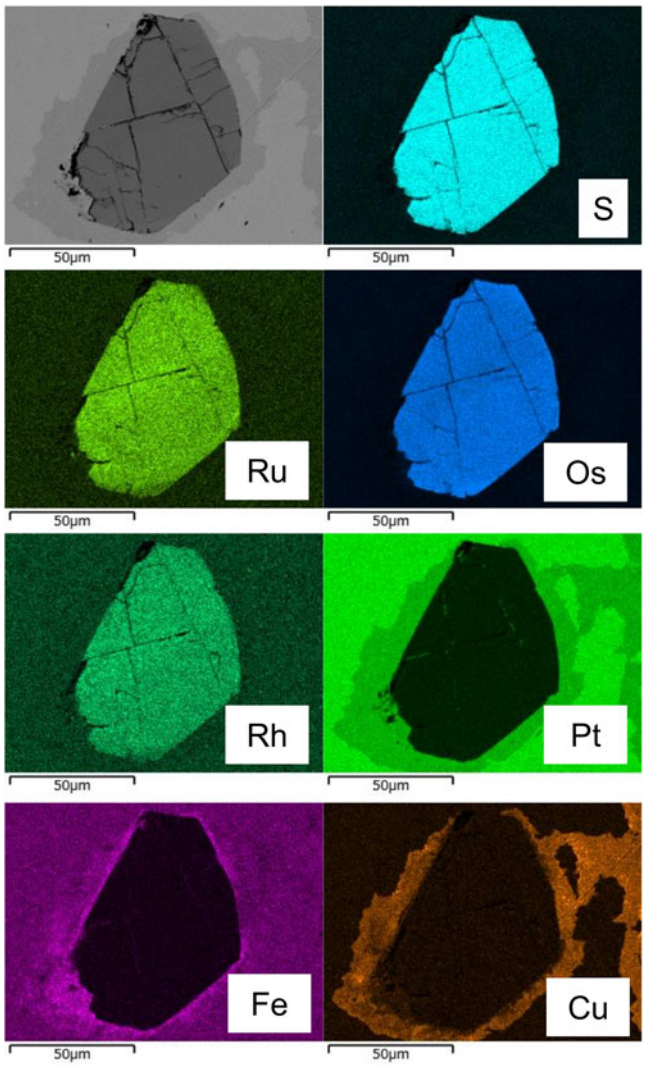

Figure. 1. Back-scattered electron image and element distribution maps of grain with an erlichmanite–laurite solid-solution composition surrounded by tulameenite and isoferroplatinum.

The isoferroplatinum from Haraigawa has a composition close to the ideal Pt_3Fe composition and commonly contains a small amount of Pd. Isoferroplatinum rims often coexist with tulameenite (Pt_2CuFe) and tetraferroplatinum (PtFe). Isoferroplatinum-based grains are accompanied by the recently discovered mineral minakawaite (RhSb) and various PGM grains, such as laurite–erlichmanite solid-solution minerals, osmium (Os), bowieite (Rh_2S_3), kingstonite (Rh_3S_4), miassite ($Rh_{17}S_{15}$), cherepanovite (RhAs), hollingworthite (RhAsS), cuprorhodsite [$(Cu,Fe)Rh_2S_4$] and irarsite (IrAsS) (Nishio-Hamane *et al.*, 2019). Grains with laurite–erlichmanite solid-solution compositions are the most abundant sulfide inclusions in isoferroplatinum-based grains and have subhedral or rounded forms, occasionally with a clear zonal texture. Bowieite (Rh_2S_3) is the second-most abundant sulfide inclusion in isoferroplatinum (Pt_3Fe) (Nishio-Hamane *et al.*, 2019). A characteristic of the placer from Haraigawa is that it is rich in Rh and produces a variety of Rh minerals.

The major and minor elements of Ir-poor laurite–erlichmanite grains with sizes ranging from several tens to ~100 micrometres were analysed using a JEOL scanning electron microscope (SEM, JSM–7001F operated at 15 kV and 1.0 nA) equipped with an Oxford energy dispersive X-ray spectroscopy at Kumamoto University, Japan. Corrections were made using the *Aztec* Oxford software. Quantitative analyses have been confirmed for many laboratory-standard compounds including synthetic platinum-group compounds such as $RuSe_2$, Rh_2S_3, $PdSb_2$ and PtP_2. The deviation from 100 wt.% in total and from the ideal number of the chemical formula obtained by specifying the number of anions was <0.5%. Relative analytical errors (1σ) of standard compounds were generally better than ~1%. Elements containing >0.1 wt.% can be detected, but the quantification is poor for elements with content <1 wt.%.

A back-scattered electron image and element-distribution maps in Fig. 1 show a rounded subhedral laurite–erlichmanite solid-solution grain from Haraigawa surrounded by tulameenite (Pt_2CuFe) and isoferroplatinum (Pt_3Fe). The laurite–erlichmanite samples from Haraigawa contained very low amounts of Ir, Pd, or Pt, and we searched for areas containing no, or the lowest Ir or Pd compared with Rh as additional components. The variation in Ru and Rh components with respect to the change in Os content in eight solid-solution grains are shown in Fig. 2.

The grains contain zoning and only small areas (several tens of μm) for each crystal were homogeneous. Single crystals were carefully selected for crystallography from homogeneous areas that contained almost no Ir. The variation in the atomic ratios of Ru, Os and Rh among the analysed points in each area was within ~1–4% (Table 1). Other elements such as Pd, Pt, As and Se were below the detection limit in each area.

Single-crystal X-ray diffraction and structure refinement

Structural analyses were performed on four single crystals (Table 2). Crystallographic data were collected on an Rigaku XtaLAB Synergy diffractometer with a HyPix6000 area detector. Systematic absences were found to be consistent with the space group $Pa\bar{3}$, and no evidence of lower symmetry was detected in any of the four crystals. The intensity of the reflection was measured using Mo*K*α radiation (0.71073 Å) focused by a mirror. The details of the data-correction method are described in the crystallographic information files, deposited with the Principal

https://doi.org/10.1180/mgm.2022.139 Published online by Cambridge University Press

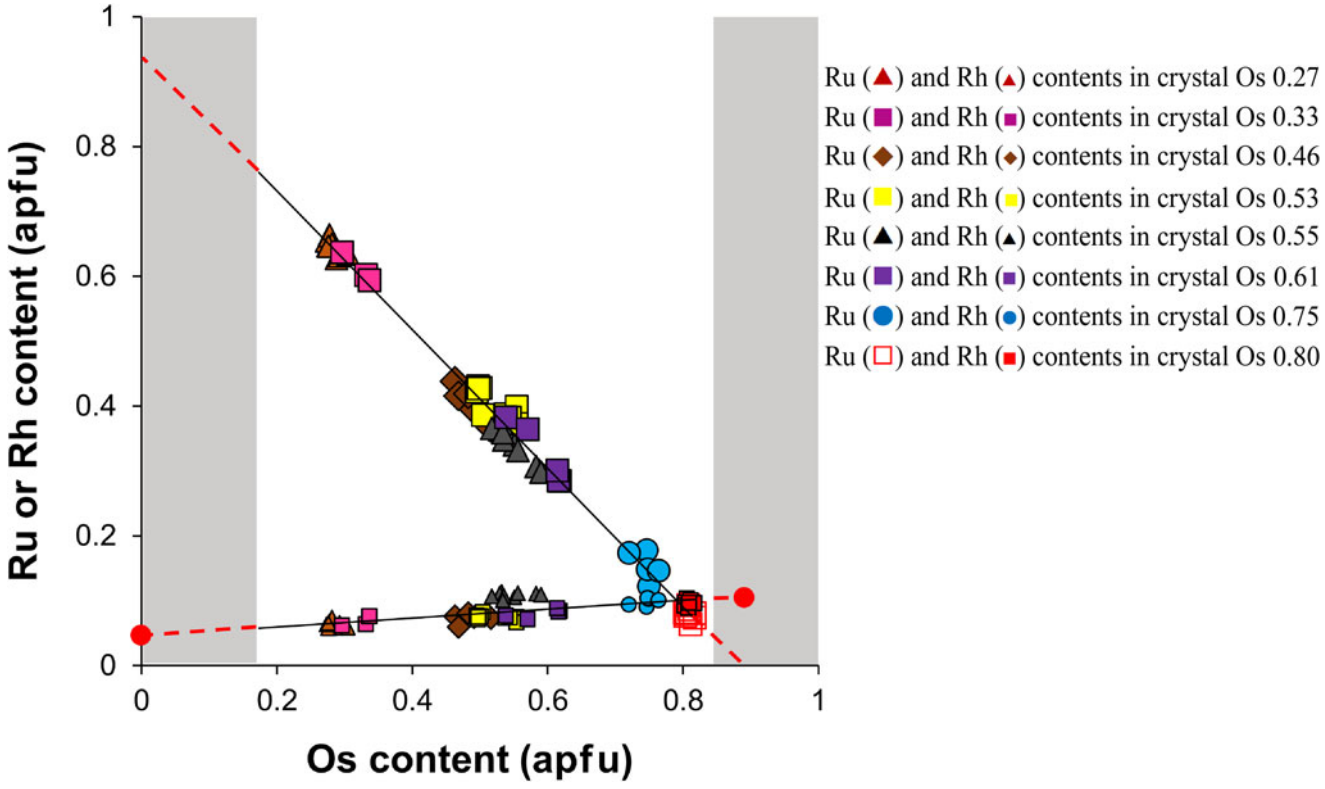

Figure. 2. Variation in Ru and Rh contents *vs*. Os (atoms per formula unit, apfu) in the erlichmanite–laurite $Os_{1-x-y}Ru_xRh_yS_2$ solid-solution series. There is no solid solution in the area shown in grey because both Ru and Rh are substituted. Red circles represent the contents of Rh at both end-members estimated by the red dashed line.

Editor of *Mineralogical Magazine* and are available as Supplementary material (see below). Independent reflections were used to refine the crystal structure using the full-matrix least-squares method in the *SHELXL* program (Sheldrick, 2015). The refinement was initiated with the positional parameters reported by Stingl *et al.* (1992). Because it is difficult to distinguish between Ru and Rh from each X-ray scattering factor, the Rh value was fixed using its average chemical analysis value, and the site occupancies of Ru and Os atoms were refined at the *M* site of each crystal. The ratio of Ru and Os at the *M* sites was refined by assuming that the rest of Rh is occupied by both Ru and Os. The following chemical formulas for the four crystals were determined from the site-occupancy refinements: $Os_{0.332(4)}Ru_{0.601(4)}Rh_{0.067(8)}S_2$; $Os_{0.457(3)}Ru_{0.467(3)}Rh_{0.076(7)}S_2$; $Os_{0.595(5)}Ru_{0.325(5)}Rh_{0.080(5)}S_2$; and $Os_{0.812(6)}Ru_{0.092(6)}Rh_{0.096(4)}S_2$. Each chemical formula obtained from site-occupancy refinement was in good agreement with the respective values obtained from chemical analysis (Table 1). The R_1 indices ($R_1 = \Sigma||F_o| - |F_c||/\Sigma|F_o|$) for the four crystals converged between 0.0071 and 0.0096, using anisotropic temperature factors. The

Table 1. Chemical compositions of the erlichmanite–laurite solid-solution specimens used for single-crystal structure analyses.

	0611-5- Os032		0611-4- Os049		0611-4- Os058		0611-1- Os081	
	(3 points)		(7 points)		(4 points)		(8 points)	
	average	range	average	range	average	range	average	range
wt.%								
S	33.59(39)	34.02–33.28	30.41(31)	32.36–29.90	30.43(1.05)	31.35–28.97	27.72(27)	28.05–27.17
Ru	31.57(1.06)	31.11–30.83	19.99(79)	21.56–19.28	14.10(1.53)	16.38–13.16	3.41(36)	3.94–2.73
Os	31.27(2.33)	33.18–28.68	43.42(1.04)	45.12–42.84	51.64(3.93)	55.13–46.53	64.52(55)	65.29–63.81
Rh	3.54(44)	4.05–3.24	3.65(28)	2.61–3.07	3.86(20)	4.07–3.58	4.16(19)	4.47–3.86
Ir	0.74(1.21)	2.14–0.00	1.42(68)	2.09–0.00	0.06(5)	0.09–0.00	0.84(1.17)	2.50–0.00
Cu	n.d.		n.d.		n.d.		0.26(34)	0.85–0.00
Fe	0.04	0.04–0.00	n.d.		n.d.		n.d.	
Total	100.72(1.48)		98.88(1.23)		100.79(3.24)		100.88(1.13)	
mol.% (S = 2)								
Ru	0.611(23)	0.637–0.594	0.425(14)	0.438–0.395	0.321(34)	0.357–0.285	0.087(9)	0.093–0.064
Os	0.321(22)	0.337–0.296	0.490(15)	0.501–0.469	0.578(39)	0.618–0.538	0.809(6)	0.817–0.802
Rh	0.067(8)	0.076–0.062	0.076(7)	0.081–0.059	0.080(5)	0.088–0.077	0.096(4)	0.103–0.089
Total	1.000(6)		0.991(22)		0.980(13)		0.997(18)	

n.d. – not detected

https://doi.org/10.1180/mgm.2022.139 Published online by Cambridge University Press

Table 2. Crystallographic data, data collection parameters, and refinement parameters for $Os_{1-x-y}Ru_xRh_yS_2$ pyrite-type erlichmanite–laurite solid solution from Haraigawa, Kumamoto.

Sample number	0611-5- Os032	0611-4- Os049	0611-4- Os058	0611-1- Os081
Temperature (K)	298(1)			
Chemical formula	$Os_{0.332}Ru_{0.601}Rh_{0.067}S_2$	$Os_{0.457}Ru_{0.467}Rh_{0.076}S_2$	$Os_{0.595}Ru_{0.325}Rh_{0.080}S_2$	$Os_{0.812}Ru_{0.092}Rh_{0.096}S_2$
Formula weight	194.90	206.08	218.37	237.81
a (Å)	5.61826(6)	5.62191(7)	5.62589(3)	5.63142(8)
V (Å^3)	177.340(6)	177.685(6)	178.063(3)	178.589(7)
Density (g/cm^3)	7.300	7.704	8.146	8.845
Z	4	4	4	4
$F_{(000)}$	346.8	363	380	408
Radiation type and wavelength (Å)	Mo$K\alpha$, 0.71073	Mo$K\alpha$, 0.71073	Mo$K\alpha$, 0.71073	Mo$K\alpha$, 0.71073
μ (mm^{-1})	31.657	39.571	47.908	61.686
Crystal size (mm)	0.040 × 0.030 × 0.018	0.037 × 0.024 × 0.017	0.031 × 0.029 × 0.020	0.044 × 0.038 × 0.027
Diffractometer	XtaLAB Synergy, Single source diffractometer with an HyPix6000 area detector			
2θ range (°)	≤ 95	≤ 95	≤ 95	≤ 95
No. of measured reflections	19,010	16,400	22,928	16,539
No. of Independent reflections	281	281	281	281
R_{int}	0.0475	0.0325	0.0515	0.0499
R_1	0.0088	0.0071	0.0087	0.0096
wR_2	0.0204	0.0145	0.0155	0.0188
Goodness of fit, S	1.083	1.139	1.106	1.101
Largest diff. peak/hole (e Å^{-3})	0.506 / −0.576	0.464 / −0.489	0.809 / −0.697	0.807 / −0.786
u-parameter (x coordinate for S)	0.38633(3)	0.38580(3)	0.38480(4)	0.38408(5)
U_{11} M (Å^2)	0.00284(4)	0.00257(3)	0.00295(4)	0.00319(4)
U_{12} M (Å^2)	−0.00005(2)	−0.00004(1)	−0.00005(2)	−0.00003(2)
U_{11} S (Å^2)	0.00405(7)	0.00390(5)	0.00435(8)	0.00480(9)
U_{12} S (Å^2)	0.00025(6)	0.00023(5)	0.00018(7)	0.00023(9)
Θ_D bulk (K)	>570	>580	>548	>523

structural refinement data and selected interatomic distances are listed in Tables 2 and 3, respectively.

Results and discussion

Rh substitution for Ru and Os in the erlichmanite–laurite solid solutions

The erlichmanite–laurite solid-solution samples from Haraigawa are characteristically Rh rich and Ir poor. The solid solutions from Haraigawa are unique in that trace amounts of Cu up to 0.85 wt.% are substituted in some crystals rich in Os (Table 1). No significant substitutions of Pd and Pt were observed in the examined grains, despite the coexistence of Pd and Pt minerals (Nishio-Hamane *et al.*, 2019) contrary to reports by Bowles *et al.* (1983) that significant amounts of Pd and Pt are dissolved.

Rhodium is present in all erlichmanite–laurite samples from Haraigawa, and its content ranges from 0.07 to 0.10 apfu (y = 0.07–0.10 in $Os_{1-x-y}Ru_xRh_yS_2$). For this reason, Os and Ru contents are limited in a range between $Os_{0.18}Ru_{0.75}Rh_{0.07}S_2$ with minimum Os and maximum Ru and $Os_{0.82}Ru_{0.08}Rh_{0.10}S_2$ with maximum Os and minimum Ru (grey shading in Fig. 2). Note that in erlichmanite component-rich solid solutions with Os > 0.80 apfu and Ru < 0.10 apfu, Rh predominates over Ru (red circle, Fig. 2). The results in the present study and the published data on the Rh-rich erlichmanite–laurite solid solution (e.g. Begizov *et al.*, 1976) suggest that Rh tends to substitute for Os slightly more than Ru.

Table 3. Selected bond distances and bond-angle variance for MS_2 pyrite-type $Os_{1-x-y}Ru_xRh_yS_2$ erlichmanite–laurite solid solution.

	0611-5-Os032	0611-4-Os049	0611-4-Os058	0611-1-Os081
M–S distances (Å)	2.35091(17)	2.35131(18)	2.3509(3)	2.3517(3)
S–S distances (Å)	2.2123(3)	2.2240(4)	2.2451(4)	2.2613(4)
(M–S)/(S–S)	1.0626	1.0572	1.0471	1.0400
Short (S···S) distance (Å)	3.1997(3)	3.1989(3)	3.1958(4)	3.1951(4)
Long (S···S) distance (Å)	3.4452(3)	3.4470(3)	3.4487(4)	3.4516(4)
Long(S···S)/ Short (S···S)	1.0767	1.0776	1.0791	1.0803
Narrow S–M–S (°)	85.77(3)	85.72(3)	85.64(3)	85.58 (4)
Wide S–M–S (°)	94.23(3)	94.28(3)	94.36(3)	94.42(4)

Compositional dependence of the unit-cell parameter

The unit-cell parameters and u parameters (u,u,u coordinate for the S atom) of the synthesised pure RuS_2 and OsS_2 are 5.6106(3)Å, 0.38831(4) (Lutz *et al.*, 1990) and 5.6194(7) Å, 0.38616(6) (Stingl *et al.*, 1992), respectively. Sutarno *et al.* (1967) also reported the unit-cell dimensions and u parameter (5.6095(5) Å, 0.3885(7) for RuS_2 and 5.6196(3) Å, 0.3864(13) for OsS_2) using the powder X-ray diffraction method. In the cases where Vegard's relationship holds, a linear composition dependence of the unit-cell parameter is observed. The unit-cell parameter of the Rh-free $Os_{1-x}Ru_xS_2$ solid solution can be expressed as:

$$[a\ (\text{Å})]^{Os_{1-x}Ru_xS_2} = x[a\ (\text{Å})]^{RuS_2} + (1-x)\cdot[a\ (\text{Å})]^{OS_2}$$

Osmium and Ru are assumed to differ in size and exhibit constant atomic/ionic radii (Denton and Ashcroft, 1991). Hence adding a constant amount of larger ions leads to an increase in the unit-cell parameter, approximately parallel to the straight line of Vegard's relationship.

The unit-cell parameters for the Rh-bearing erlichmanite–laurite solid solutions from Haraigawa change from 5.61826(6) Å to 5.63142(8) Å (Fig. 3a and b), which is very different from

https://doi.org/10.1180/mgm.2022.139 Published online by Cambridge University Press

the change expected from Vegard's law using the data of these end-member components. On the RuS_2-rich side, ($v = 0$ or $w = 1$), although the Rh content was ~7 at.%, the projected data line shows no large change in the unit-cell parameter. On the OsS_2-rich side, a much larger increase in the unit-cell parameter was observed than expected by Vegard's law. Although the Rh substitution of Os has a significantly different effect on the crystal structure than that of Ru substitution, a linear relationship was observed in Fig. 3a and b.

The composition without Os of $(Ru_{0.95}Rh_{0.05})S_2$ can be estimated from extrapolation in Fig. 2 (the extrapolated values of Ru and Rh crossing the point Os = 0) and without Ru of $(Os_{0.90}Rh_{0.10})S_2$ (the extrapolated value where the Rh line crosses the x axis, where Ru = 0). Then the effect of the Rh content on the unit-cell parameters in $(Ru_{0.95}Rh_{0.05})S_2$ can be estimated by extrapolating the best fit line for the solid-solution samples (diamonds) in Fig. 3a to Os = 0.0 ($v = 0$). This gives the value of 5.609 Å which is thus due to 5 at.% Rh in RuS_2 i.e. $(Ru_{0.95}Rh_{0.05})S_2$, which is 0.0016 Å smaller than that (5.6106(3) Å) for pure RuS_2. Applying Vegard's law (0.0016 Å is multiplied by 20.0, and subtract from that for RuS_2) gives $a = 5.579$ Å for the hypothetical RhS_2. This value is close to the value of 5.58 Å given previously for pyrite-type RhS_2 by Thomassen (1929).

The value of 5.633 Å due to $(Os_{0.90}Rh_{0.10})S_2$, i.e. 10 at.% Rh in OsS_2 can be estimated by similar extrapolation of the compositional changes to Ru = 0.0 ($w = 0$) in Fig. 3b, and it differs by 0.0136 Å from that (5.6194(7) Å) for pure OsS_2. If Vegard's law is applied (0.0136 Å is multiplied by 10.0, and added to that for OsS_2), $a = 5.755$ Å is obtained as the unit-cell parameter of hypothetical pure RhS_2. This value is as large as the unit-cell parameter of 5.73 Å for the hypothetical pyrite-type RhS_2 phase derived by Hulliger (1964). Conflicting unit-cell parameters have been reported for RhS_2 (Thomassen, 1929; Hulliger, 1964). No single-crystal structure analysis of pyrite-type RhS_2 has been reported so

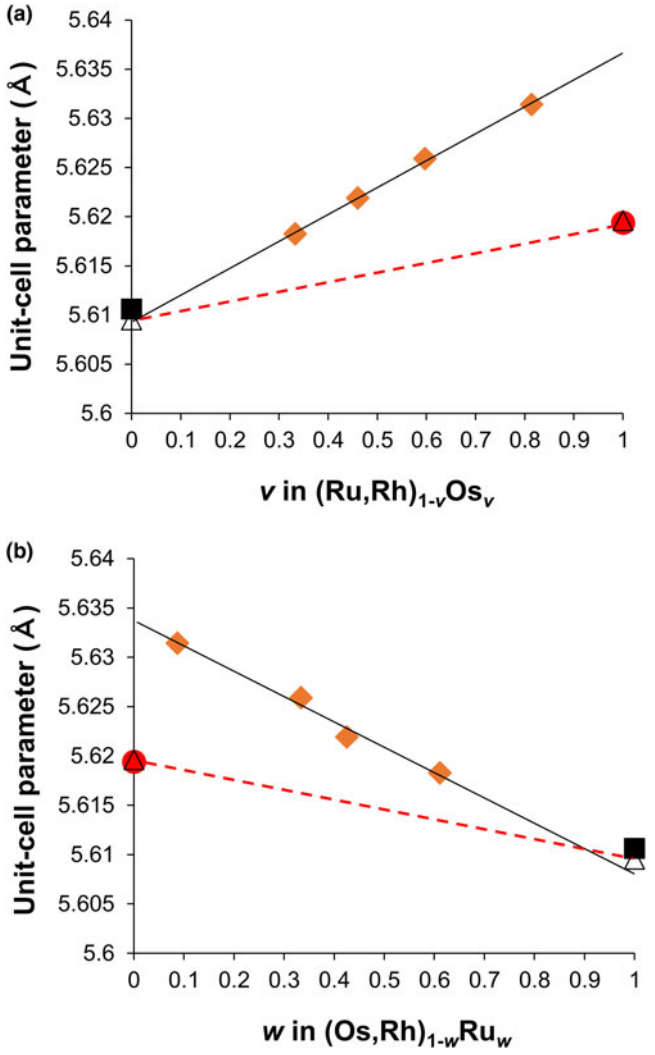

Figure. 3. Compositional dependences of unit-cell parameters: (a) v in $(Ru,Rh)_{1-v}Os_v$ and (b) w in $(Os,Rh)_{1-w}Ru_w$ in the erlichmanite–laurite $Os_{1-x-y}Ru_xRh_yS_2$ solid solutions ($x = 0.09$–0.60 and $y = 0.07$–0.10), as orange diamonds. The end-members of both series ($v = 0$, RuS_2, $v = 1$, OsS_2; and $w = 0$, OsS_2, $w = 1$, RuS_2) are shown for comparison. Data from: White triangles – Sutarno *et al.* (1967); black square – Lutz *et al.* (1990); and red circle – Stingl *et al.* (1992). The red dashed line shows the change expected from Vegard's Law for $Os_{1-x}Ru_xS_2$ solid solutions.

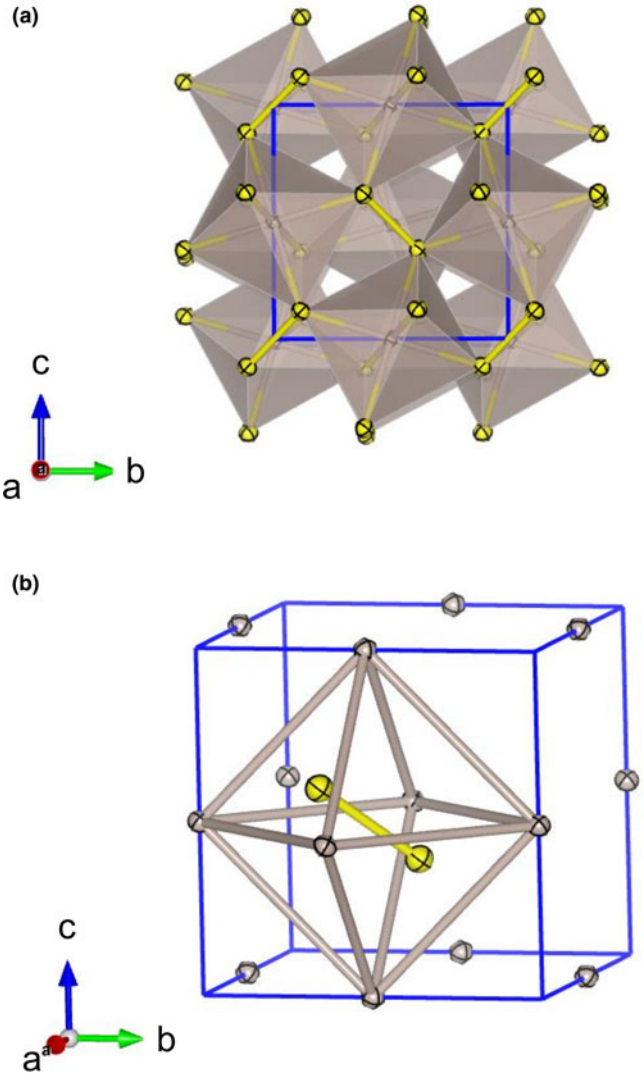

Figure. 4. (a) The crystal structure of $Os_{0.81}Ru_{0.09}Rh_{0.10}S_2$ erlichmanite, viewed parallel to the a-axis. The S–S bond is shown in the middle of the unit cell. (b) The $(S_2)M_6$ octahedron around S_2 and M cations are located at the face-centred cubic sub-unit. Each S ion bonds with one S ion (S–S: 2.2613(4) Å) and three M cations (M–S: 2.3517(3) Å). Atomic displacement ellipsoids are drawn for the 99% probability level. The crystal structures were illustrated using *VESTA* (Momma and Izumi, 2011).

https://doi.org/10.1180/mgm.2022.139 Published online by Cambridge University Press

far. Pyrite-type RhS_2 has not been observed in high-temperature regions under normal pressure (Parthé *et al.*, 1967; Foise *et al.*, 1983). Pyrite-type $RhSe_2$ ($a = 5.9336(4)$; Geller and Cetlin, 1955) and CoS_2 ($a = 5.5385(2)$; Nowack *et al.*, 1991) exist, and pyrite-type $IrS_{1.9}$ has been synthesised ($a = 5.68$ Å) at 6 GPa and 1500°C by Munson (1968). Many stable platinum-group chalcogenides have pyrite-type structures (Furuseth *et al.*, 1965; Sutarno *et al.*, 1967; Stassen and Heyding, 1968; Tokuda *et al.*, 2019).

Structure distortion and S–S distance in $Os_{1-x-y}Ru_xRh_yS_2$ solid solution

Laurite and erlichmanite have S_2 sub-units (S_2^{2-}, disulfide ion). The pyrite-type structure MS_2 is closely related to the NaCl-type structure. The S_2 groups (connected by covalent bonds) and M cations in the pyrite-type structure are arranged in the anion and cation sites of the NaCl-type structure, respectively. M cations form a face-centred cubic sublattice (Fig. 4). The M cation is bound to six S atoms in the six S_2 groups. The S_2 groups are arranged along the three-fold rotoinversion axes of a lower class of cubic symmetry (the space group $Pa\bar{3}$), which run in the direction of the body diagonals of the cell and do not intersect each other. Thus, the pyrite-type structure of MS_2 is a three-dimensional assembly of corner-sharing MS_6 octahedra, wherein the M cation is bound to only one S ion in the S_2 group, and each S anion is common to three octahedra.

The polyhedron around the X_2 group forms an undistorted $(X_2)M_6$ octahedron (Fig. 4b). Cation M is located at the origin of the face-centred cubic sub-unit and has no degrees of freedom with respect to its atomic coordinates. Interestingly, this octahedron has an unusually high symmetry as a local structure, and exhibits no structural relaxation owing to electrostatic repulsion. The S anion site is at the Wyckoff position 8*c*, and the atomic coordinates of the S anion are specified by a single u parameter (u, u, u coordinates). The S anions possess a degree of freedom only in the direction of the body diagonals, that is, in the (u, u, u) direction. In pyrite-type compounds, the arrangement of atoms for structural optimisation must be achieved using only two parameters, the unit-cell parameter a and the parameter u. The unit-cell parameter a increases whereas the u parameter decreases with increasing Os contents in the solid solutions (Table 1).

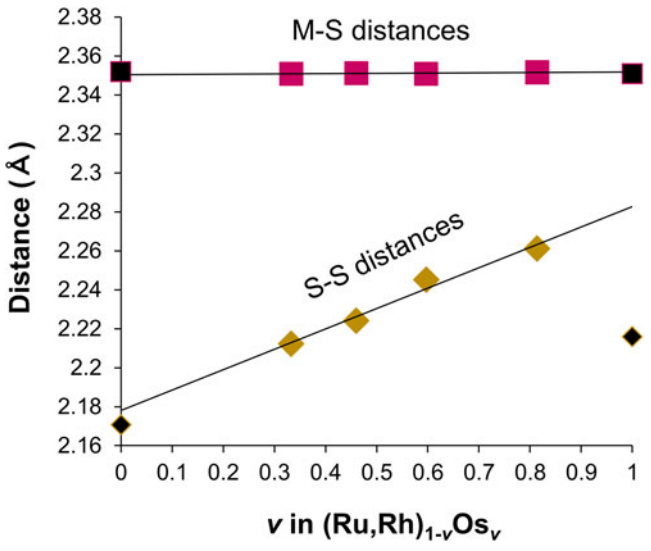

Figure. 5. Compositional dependences in M–S and S–S bonding distances with respect to Os content in the erlichmanite–laurite solid solutions ($Os_{1-x-y}Ru_xRh_yS_2$) ($y = 0.07$–0.10). Both series end-members are shown with dark symbols.

Owing to the symmetry of the S site, the freedom of atomic coordinates (u parameter) of the S atoms is limited to vary only along the three-fold rotoinversion axis. For the same unit-cell parameters, the M–S distance decreased, and the molecular distance S–S increased as the u parameter decreased. Hence, a decrease in the u parameter leads to a decrease in the (M–S)/(S–S) ratio. Decreasing the u parameter also leads to an increase in the long(S···S)/short(S···S) ratio. Similarly, compounds with smaller u parameters exhibit an increased angle variance for the MS_6 octahedron (Tables 2, 3). The differences between the long S···S distance and the short S···S or between the narrow S–M–S angle and the wide S–M–S angle increase with increasing Os content (Table 3). The FeS_6 octahedra in FeS_2 pyrite ((Fe–S)/(S–S) = 1.0475(5), long(S···S)/short(S···S) = 1.0791, S–Fe–S(1) = 85.64(4)° and S–Fe–S(2) = 94.36(4)°; Tokuda *et al.* (2019) had exactly the same distortion (Table 3) as that in the $Os_{0.60}Ru_{0.32}Rh_{0.08}S_2$ solid solution from Haraigawa samples.

Owing to the low degree of freedom for structural changes, crystal stabilisation involves a unique chemical bonding state with higher energy, which is rare in other structures. In many cases, unusual chemical bonding occurs to achieve a three-dimensional periodicity and acceptable M–S distances. In pyrite, all electrons in the low-spin state Fe^{2+} occupy t_{2g} orbitals ($S = 0$), which is a biased electronic arrangement. In terms of transition metal ions, the energy of the low-spin state is always higher than that of the high-spin state. The number of electrons in the d-orbital increases to d^6, d^7 and d^8 across the first transition metal period for Fe^{2+}, Co^{2+} and Ni^{2+} respectively. The radii of Fe^{2+} and Co^{2+} in the low-spin state are 0.61 and 0.65 Å, respectively (Shannon, 1976). The size difference between Fe^{2+} and Co^{2+} is 0.04 Å. In sulfides, the bond between each cation and the sulfide ion has both ionic and covalent characteristics, and the spin state of the transition metal ion can change. For Rh, Rh and Os, ionic (Pauling, 1940; Shannon *et al.*, 1981), covalent (Pauling, 1940; Cordero *et al.*, 2008) and metallic (Pauling, 1940) radii have been proposed corresponding to their respective bonding states. Size differences of 0.006 to 0.04 Å are expected among these elements, even though their bonding characteristics are similar. Curiously, the M–S distances in the solid-solution minerals from Haraigawa showed little variation (Fig. 5; Table 3). The chemical bonding characteristics of the atoms cannot be interpreted from the published interatomic distances.

The compositional dependence of the M–S and S–S distances in the Rh-bearing erlichmanite–laurite solid solution from Haraigawa, and those of pure RuS_2 (Lutz *et al.*, 1990) and OsS_2 (Stingl *et al.*, 1992) are shown in Fig. 5. A unique compositional dependence of the distances was observed as a structural change in the solid solution. The unit-cell parameters of pure RuS_2 and OsS_2 are different (Fig. 3). However, the M–S distances in the $Os_{1-x-y}Ru_xRh_yS_2$ system, including the solid solutions containing Rh, changed by only 0.001 Å (Table 3). In contrast, the S–S distances change significantly, and the difference between them reaches 0.1 Å. These changes are essential phenomena that occur in this system, even when comparing the values of pure RuS_2 and OsS_2. Moreover, the unique feature of this solid solution containing ~10 at.% Rh is the peculiar increase in the S–S distance in the solid solution containing a substantial amount of

https://doi.org/10.1180/mgm.2022.139 Published online by Cambridge University Press

Os (Fig. 5). The elongations of the S–S distance are not very large in Ru-rich solid solutions ($Os_{0.33}Ru_{0.60}Rh_{0.07}S_2$), although they contain 7 at.% Rh (Table 3). In Fig. 5, a linear relationship between the S–S distance and the change in Os content can be seen in the $Os_{1-x-y}Ru_xRh_yS_2$ solid solution ($y = 0.07$–0.10). A negligible effect of Rh substitution in RuS_2 was observed with respect to the S–S distance, whereas the effect of Rh substitution on OsS_2 was extremely large. The Rh substitution of Ru in RuS_2 and the Rh substitution of Os in OsS_2 have very different effects on the S–S distance, that is, on the chemical bonding characteristics of the anions. The change in covalent character at the S–S bond seems to eliminate the size effect of the cation itself.

Because the *M*–S interaction is greater for low-spin compounds, S may be attracted strongly to low-spin metals. The longer S–S distance implies a decrease in covalent character at the S–S bond in pyrite-type MS_2 compounds. The delocalisation of the electrons in the S_2 group weakens the molecular S–S bond.

The S–S bond in NiS_2 (2.065 Å, Nowack *et al.*, 1991), which is the minimum among pyrite-type sulfides, is almost equivalent to the S–S single bond (2.06 Å) in a disulfur molecule (S_2) and the S–S distance (2.055(2) Å) in elemental solid sulphur (Rettig and Trotter, 1987). The S–S distance in RuS_2 (2.1707(8) Å, Lutz, 1990) is even longer than the S–S distance in NiS_2, which demonstrates an increase in ionicity and a decrease in covalent bonding character in S–S bonds. The S–S distance in OsS_2 (2.2160(12) Å, Stingl *et al.*, 1992) is significantly larger than that in RuS_2 (2.1707(8) Å), FeS_2 (2.1618(9) Å, Tokuda *et al.*, 2019) and CoS_2 (2.124 Å, Nowack *et al.*, 1991). In OsS_2, the ionicity of the S–S bond further increased compared to that of FeS_2 and RuS_2. The S–S distance was even longer in the $Os_{0.81}Ru_{0.09}Rh_{0.10}S_2$ erlichmanite than in OsS_2 (Fig. 5). The molecular S–S distances in the laurite–erlichmanite solid solutions were longer than those in other pyrite-type compounds (Tokuda *et al.*, 2019). The *M*–S distances in OsS_2 (2.3510(5) Å) and RuS_2 (2.3520(3) Å) are the same, and the Fe–S distance in FeS_2 was 2.264 (1) Å. A unique change in the bonding distances occurs in pyrite-type sulfides of Fe, Ru and Os belonging to the same group in the periodic table. The (*M*–S)/(S–S) ratios decreased with increasing Os content, as listed in Table 3, suggesting a corresponding decrease in the bond strength of the S_2 groups. The increase in electron transfer from cations to S–S molecules in the $Os_{0.81}Ru_{0.09}Rh_{0.10}S_2$ erlichmanite is one of the factors responsible for the elongation of the S–S bond distances. Furthermore, the fact that the *M*–S distance does not change even when the neighbouring group is replaced by 10 at.% Rh indicates a change in the bonding characteristics of the Os–S, Ru–S, and Rh–S bonds from the standard states. Thus, we conclude that the factor that lowers the total energy in pyrite-type crystals is mainly controlled by anions.

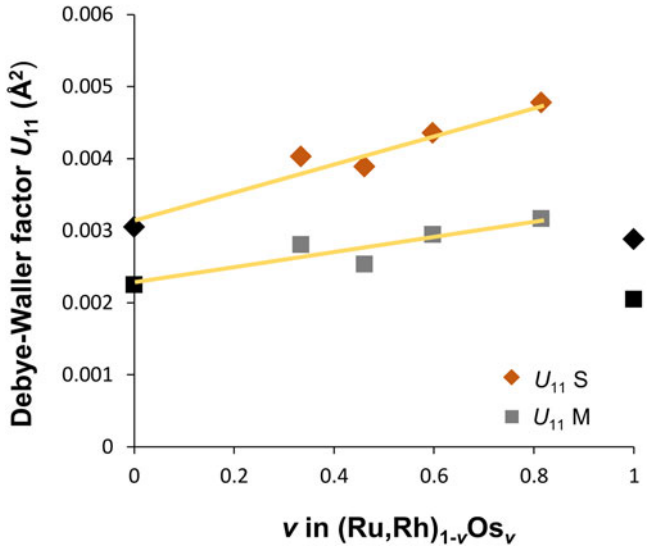

Figure. 6. Variation of Debye–Waller factor U_{11} against Os component in the erlichmanite–laurite $Os_{1-x-y}Ru_xRh_yS_2$ solid solutions ($y = 0.07$–0.10). End-members RuS_2 and OsS_2 (0.00205(3) Å^2 *M* site and 0.00288(6) Å^2 *S* site) are shown with dark symbols.

Debye–Waller factor and static disorder in the solid solutions

The Debye–Waller factors obtained from the diffraction experiments include the effects of static and dynamic disorders. Static disorder is a configurational disorder, whereas dynamic disorder arises from the thermal vibrations of atoms. In the case of a solid solution, a static disorder component is always included. The compositional dependence of the Debye–Waller factor U_{11} in solid solutions from Haraigawa is shown in Fig. 6 as it increases with an increase in the Os component (Fig. 6; Table 2). It can be seen that the effect of Rh on the Debye–Waller factor is different for Os and Ru substitutions. A large increase in the Debye–Waller factor occurs at 10 at.% Rh in Os-rich solid solutions, whereas no large effect occurs even at ~7 at.% Rh in Ru-rich solid solutions (Table 2). In the $Os_{0.81}Ru_{0.09}Rh_{0.10}S_2$ erlichmanite, U_{11} (0.00319(4) Å^2) for the *M* site increases by 0.0011 Å^2 and U_{11} (0.00480(9) Å^2) for the S site increases by 0.0019 Å^2 compared to those for pure OsS_2 (0.00205(3) Å^2 and 0.00288(6) Å^2, respectively, black symbols). The root-mean-square displacements (RMSD) for *M* and S sites (0.0565 Å and 0.0693 Å) in $Os_{0.81}Ru_{0.09}Rh_{0.10}S_2$ increase by 0.0112 Å and 0.0156 Å, respectively. The amplitude due to the thermal vibration is dominant in pure OsS_2. The value of 0.0156 Å is approximately a quarter of the RMSD (0.0537 Å) for the S atom in OsS_2. This value is approximately one-third of the increase in the S–S distance (0.045 Å) observed in the solid solution. We conclude that the increase in the S–S distance by the Rh replacement of Os with only several percent in the Rh-bearing erlichmanite–laurite solid solutions reflects the change in S–S bonding characteristics throughout the crystal. The substitution of some Os by Rh affects all (Os, Ru, Rh)–S bonds.

Atomic displacement ellipsoids of the *M* (*M*: $Os_{0.81}Ru_{0.09}Rh_{0.10}$) and S sites in the $Os_{0.81}Ru_{0.09}Rh_{0.10}S_2$ erlichmanite are shown in Fig. 4. The atomic displacement ellipsoids of both *M* and S are effectively spherical, and no elongation along the *M*–S and S–S bond directions was observed. Based on the site-symmetry restrictions, U_{12}, U_{13} and U_{23} are equivalent; therefore, changes to these parameters results in the distortion of the atomic displacement ellipsoid along [111], which is parallel to the S–S bond. The U_{12} parameters of the S sites in MS_2 have the same positive value of ~0.0002 Å^2 for all anions, and the degree of deformation from a sphere is slightly larger in $Os_{0.81}Ru_{0.09}Rh_{0.10}S_2$ erlichmanite. The atomic displacement ellipsoids for S are almost spherical ($U_{12} = 0$ indicates a sphere), implying that few static atomic displacements in specific directions are observed in the solid-solution system.

Debye temperature of erlichmanite–laurite solid solution and effect of Rh substitution

The Debye temperature Θ_D corresponding to the atom at each crystallographically equivalent site can be estimated using the

https://doi.org/10.1180/mgm.2022.139 Published online by Cambridge University Press

dynamic part of the Debye–Waller factor based on the Debye approximation (Willis and Pryor, 1975; Wood *et al.*, 2002; Yoshiasa *et al.*, 2016; Yoshiasa *et al.*, 2021). We estimated Θ_D for each atom in the site occupied solely by Ru, Os, or S using the values of U_{11} under the assumption of no configurational disorder of the atoms in pure RuS_2 and pure OsS_2. The values of Θ_D calculated for Ru and S in RuS_2 are 434 K and 661 K, respectively, using the data obtained by Lutz *et al.* (1990). The Θ_D values for Os and S in OsS_2 are 335 K and 688 K respectively, using data from Stingl *et al.* (1992). The Debye temperature for the site with the highest value in the crystal corresponds to the bulk Debye temperature of the compound (Tokuda *et al.*, 2019; Yoshiasa *et al.*, 2021). The bulk Debye temperatures Θ_D for RuS_2 and OsS_2 are estimated to be 661 and 688 K, respectively. These values are extremely high among the many known sulfides. The Debye temperature is a physical index that can be used to compare materials with different compositions. The Debye temperature is related to the melting temperature, formation temperature, thermal conductivity, atomic diffusion and hardness of the materials. Laurite (RuS_2) is the best-known hard sulfide mineral (hardness = 7.5). Bowles (1983) showed that the microindentation hardness of the laurite–erlichmanite solid-solution minerals are considerably higher than that of other sulfide minerals. González-Jiménez *et al.* (2009) attributed the preservation of laurite–erlichmanite zoning to the low diffusion coefficient of Ru and Os in pyrite-type structures. The high hardness and low diffusion coefficient of the laurite–erlichmanite series minerals are in good agreement with the calculated Debye temperatures.

The Debye temperatures of RuS_2 (661 K) and OsS_2 (688 K) are similar to those of the upper mantle constituent silicate end-member minerals, such as diopside (668 K; Levien *et al.*, 1979), enstatite (732 K; Weidner *et al.*, 1978), forsterite (758 K; Sumino *et al.*, 1977) and fayalite (507 K; Sumino, 1979). Some laurite–erlichmanite grains occurring in sealed inclusions of chromite are of magmatic origin. The euhedral shape of the laurite crystals and their sporadic distribution even within the same pod strongly suggest that laurite represents a high-temperature phase on the liquidus of primitive magma (Ahmed and Arai, 2003; Arai, 2012). In particular, laurite acts as a nucleus for the early formation of chromian spinel and silicate crystals (Tredoux *et al.*, 1995). Laurite–erlichmanite minerals form at a very high temperature (~1250°C; Brenan and Andrews, 2001). Our synthetic experiments without flux under vacuum conditions (Unoki *et al.*, 2021; Yoshiasa *et al.*, 2021) indicated that RuS_2 and $RuSe_2$ crystals did not melt nor grow, even at 1300°C.

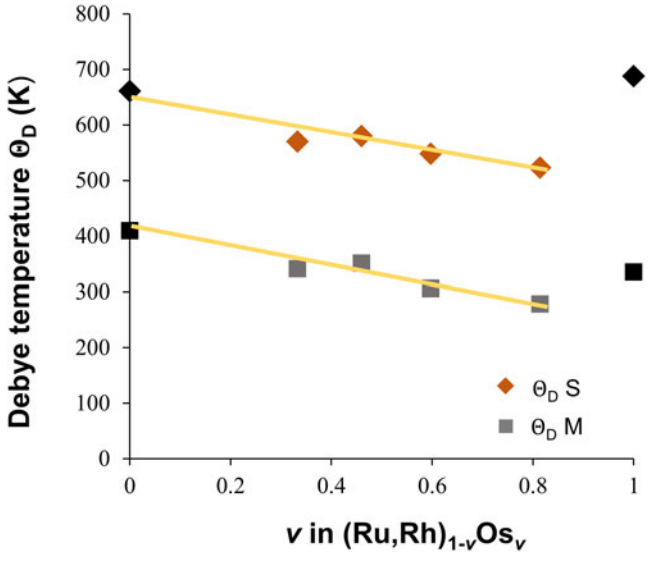

Figure. 7. Debye temperatures *vs*. Os component of cation and sulfide ion sites in the erlichmanite–laurite $Os_{1-x-y}Ru_xRh_yS_2$ solid solutions (y = 0.07–0.10). End-members are shown with dark symbols.

Several researchers (Stockman and Hlava, 1984; Augé and Johan, 1988; Melcher *et al.*, 1997; Garuti *et al.*, 1999a; Brenan and Andrews, 2001) have reported that a progressive increase in the Os content of laurite on crystallisation (Os solubility in laurite) has the effect of both lowering temperature and increasing f_{S_2}. Laurite is composed of nearly pure RuS_2 with low concentrations of Os and Ir at high temperatures and low f_{S_2} (Brenan and Andrews, 2001). When f_{S_2} increases in the melt, laurite–erlichmanite solid solutions are formed by the reaction of Ru and Os components in magma, or previously formed Ru–Os alloys with sulfur. Bockrath *et al.* (2004) considered that the origin of zoning in the solid solution was interpreted mainly as a result of changes in f_{S_2} and, to a lesser extent, in melt temperature. The bulk Debye temperature of OsS_2 is higher than that of RuS_2. This indicates that the melting temperature of erlichmanite is higher than that of laurite. The melting points of Ru, Os, Rh and Ir are 2310, 3045, 1965 and 2410°C, respectively. The high melting point of Os metal and the high Debye temperature of OsS_2 do not explain the crystallisation of Ru-rich solid solutions and RuS_2 before those of the Os-rich solid solutions and OsS_2. We therefore conclude that f_{S_2} is the main cause of laurite crystallisation prior to erlichmanite.

Contrary to the expectations from the position of the elements in the periodic table, the substitution of Ir is preceded by Ru compared to Os in petrological observations. This also depends on the effect of f_{S_2}. Because Ru is more easily sulfurised than Os and crystallises faster, Ir can be incorporated into laurite. Various Rh-rich minerals, such as Rh_3S_4 and Rh_2S_3, which show the diversity of f_{S_2}, are observed along with the laurite–erlichmanite solid-solution minerals in samples from Haraigawa. It is very likely that there were fluctuations in f_{S_2} in the magma chamber. Precipitation of PGE arsenide and PGE antimonide was also observed (Nishio-Hamane *et al.*, 2019). The f_{S_2} value in the magma increases as silicate crystals accumulate. The increase in f_{S_2} appears to induce the precipitation of Rh-rich platinum-group sulfide minerals. In the Haraigawa samples bowieite (Rh_2S_3) is the second most abundant sulfide inclusion, and irarsite (IrAsS) is also commonly observed in isoferroplatinum (Pt_3Fe).

The estimated values of 523–580 K (Fig. 7; Table 2) for the solid solutions are sufficiently large Debye temperatures for sulfides. The true bulk Debye temperature for solid solutions should be higher than the estimated value because the static effect increases the Debye–Waller factor and reduces the Debye temperature value. The Debye–Waller factors U_{11} and Debye temperatures of the solid solutions (Figs 6 and 7) exhibit a trend including pure RuS_2, however extrapolation of each trend deviates significantly from its respective value of OsS_2 (dark symbols in Figs 6 and 7). Substitution of Ru by Os with 10 at.% Rh significantly lowered the Debye temperature by as much as 170 K. Our comparison of the Debye temperature of each end-member indicated that the melting temperature of erlichmanite (688 K) is higher than that of laurite (661 K). On the other hand, the results show that the presence of several percent Rh lowers the melting point of erlichmanite solid solution compared to that of

https://doi.org/10.1180/mgm.2022.139 Published online by Cambridge University Press

the laurite solid solution. The present study revealed a significant effect of the minor component Rh on the thermal stability of OsS_2 and that these effects were significantly different between OsS_2 and RuS_2. It is shown that the effect of a minor element on physical properties is different even in the same structure with similar composition. In the erlichmanite–laurite solid-solution system, a small amount of Ir may also have some effect on physical properties.

Acknowledgements. Critical comments from Dr. Oxana Karimova (Russian Academy of Sciences), Prof. Peter Leverett (Structural Editor) and two anonymous reviewers are gratefully acknowledged. This research was partially supported by the JST SPRING (Grant Number JPMJSP2127) and JSPS KAKENHI (Grant Numbers JP18H05456 and JP20H00189). This study was performed under the guidance of the Photon Factory (PAC Nos.2015G505 and 2015G506).

Supplementary material. The supplementary material for this article can be found at https://doi.org/10.1180/mgm.2022.139

Competing interests. The authors declare none.

References

Ahmed A.H. and Arai S. (2003) Platinum-group minerals in podiform chromitites of the Oman ophiolite. *The Canadian Mineralogist*, **41**, 597–616.

Andrews D.R.A. and Brenan J.M. (2002) Phase-equilibrium constraints on the magmatic origin of laurite+ Ru–Os–Ir alloy. *The Canadian Mineralogist*, **40**, 1705–1716.

Arai S. (2012) Podiform chromitites possibly recycled within the mantle. *Japanese Magazine of Mineralogical and Petrological Sciences*, **41**, 247–256.

Arai S., Prichard H.M., Matsumoto I. and Fisher P.C. (1999) Platinum-group minerals in podiform chromitite from the Kamuikotan Zone, Hokkaido, Northern Japan. *Resource Geology*, **49**, 39–47.

Arculus R.J. and Delano J.W. (1981) Siderophile element abundances in the upper mantle: evidence for a sulfide signature and equilibrium with the core. *Geochimica et Cosmochimica Acta*, **45**, 1331–1343.

Augé T. (1985) Platinum-group-mineral inclusions in ophiolitic chromitite from the Vourinos Complex, Greece. *The Canadian Mineralogist*, **23**, 163–171.

Augé T. and Johan Z. (1988) Comparative study of chromite deposits from Troodos, Vourinos, North Oman and New Caledonia ophiolites. Pp. 267–288 in: *Mineral Deposits within the European Community* (J. Boissonnas and P. Omenetto, editors). Springer Berlin-Heidelberg, Berlin.

Begizov V.D., Zavyalov E.N. and Khvostova V.P. (1976) Minerals of the erlichmanite–laurite and hollingworthite irarsite series from Ural placers. *Zapiski Vsesoyuznogo Mineralogicheskogo Obshchestva*, **105**, 213–218.

Bockrath C., Ballhaus C. and Holzheid A. (2004) Stabilities of laurite RuS_2 and monosulfide liquid solution at magmatic temperature. *Chemical Geology*, **208**, 265–271.

Bowles J.F.W., Atkin D., Lambert J.L.M., Deans T. and Phillips R. (1983) The chemistry, reflectance, and cell size of the erlichmanite (OsS_2)-laurite (RuS_2) series. *Mineralogical Magazine*, **47**, 465–471.

Brenan J.M. and Andrews D. (2001) High-temperature stability of laurite and Ru–Os–Ir alloy and their role in PGE fractionation in mafic magmas. *The Canadian Mineralogist*, **39**, 341–360.

Cabri L.J. (2002) *The Geology, Geochemistry, Mineralogy and Mineral Benefication of Platinum-Group Elements*. Canadian Institute of Mining, Metallurgy and Petroleum, Canada.

Cordero B., Gómez V., Platero-Prats A.E., Revés M., Echeverría J., Cremades E., Barragán F. and Alvarez S. (2008) Covalent radii revisited. *Dalton Transactions*, **2008**, 2832–2838.

Corrivaux L. and Gilles Laflamme J.H. (1990) Mineralogie des elements du groupe du platine dans les chromitites de l'ophiolite de Thetford Mines, Quebec. *The Canadian Mineralogist*, **28**, 579–595.

Denton A.R. and Ashcroft N.W. (1991) Vegard's law. *Physical Review*, **A43**, 3161–3164.

Elliott N. (1960) Interatomic distances in FeS_2, CoS_2, and NiS_2. *Journal of Chemical Physics*, **33**, 903–905.

Ferrario A. and Garuti G. (1990) Platinum-group mineral inclusions in chromitites of the Finero mafic-ultramafic complex (Ivrea-Zone, Italy). *Mineralogy and Petrology*, **41**, 125–143.

Foise J., Kim K., Covino J., Dwight K., Wold A., Chianelli R. and Passeretti J. (1983) Preparation and properties of the systems cobalt ruthenium sulfide ($Co_{1-x}Ru_xS_2$) and rhodium ruthenium sulfide ($Rh_{1-x}Ru_xS_2$). *Inorganic Chemistry*, **22**, 61–63.

Folmer J.C.W., Jellinek F. and Calis G.H.M. (1988) The electronic structure of pyrites, particularly CuS_2 and $Fe_{1-x}CuxSe_2$: An XPS and Mössbauer study. *Journal of Solid State Chemistry*, **72**, 137–144.

Furuseth S., Selte K. and Kjekshus A. (1965) Redetermined Crystal Structures of $PdAs_2$, $PdSb_2$, PtP_2, $PtAs_2$, $PtSb_2$, *a*-$PtBi_2$, and $AuSb_2$. *Acta Chemica Scandinavica*, **19**, 735–741.

Garuti G., Gazzotti M. and Torres-Ruiz J. (1995) Iridium, rhodium, and platinum sulfides in chromitites from the ultramafic massifs of Finero, Italy, and Ojen, Spain. *The Canadian Mineralogist*, **33**, 509–520.

Garuti G., Zaccarini F. and Economou-Eliopoulos M. (1999a) Paragenesis and composition of laurite from chromitites of Othrys (Greece): implications for Os-Ru fractionation in ophiolitic upper mantle of the Balkan peninsula. *Mineralium Deposita*, **34**, 312–319.

Garuti G., Zaccarini F., Moloshag V. and Alimov V. (1999b) Platinum-group minerals as indicators of sulfur fugacity in ophiolitic upper mantle; an example from chromitites of the Ray-Iz ultramafic complex, Polar Urals, Russia. *The Canadian Mineralogist*, **37**, 1099–1115.

Geller S. and Cetlin B.B. (1955) The crystal structure of $RhSe_2$. *Acta Crystallographica*, **8**, 272–274.

Gervilla F., Proenza J.A., Frei R., González-Jiménez J.M., Garrido C.J., Melgarejo J.C., Meibom A., Díaz-Martínez R. and Lavaut W. (2005) Distribution of platinum-group elements and Os isotopes in chromite ores from Mayarí-Baracoa Ophiolitic Belt (eastern Cuba). *Contributions to Mineralogy and Petrology*, **150**, 589–607.

Goldschmidt V.M. (1937) The principles of distribution of chemical elements in minerals and rocks. The seventh Hugo Müller Lecture, delivered before the Chemical Society on March 17th, 1937. *Journal of the Chemical Society (Resumed)*, **1937**, 655–673.

González-Jiménez J.M., Gervilla F., Kerestedjian T. and Proenza J.A. (2007) Postmagmatic evolution of platinum-group and base-metal mineral assemblages in Palaeozoic ophiolitic chromitites from the Dobromirtsi massif, Rhodope Mountains (SE Bulgaria). Pp. 889–892 in: *Biennial Meeting of the Society for Geology Applied to Mineral Deposits*. Dublin, Ireland.

González-Jiménez J.M., Gervilla F., Proenza J.A., Kerestedjian T., Augé T. and Bailly L. (2009) Zoning of laurite (RuS_2)–erlichmanite (OsS_2): implications for the origin of PGM in ophiolite chromitites. *European Journal of Mineralogy*, **21**, 419–432.

Harris D.C. (1974) Ruthenarsenite and iridarsenite, two new minerals from the Territory of Papua and New Guinea and associated irarsite, laurite and cubic iron-bearing platinum. *The Canadian Mineralogist*, **12**, 280–284.

Harris D.C. and Cabri L.J. (1991) Nomenclature of platinum-group-element alloys; review and revision. *The Canadian Mineralogist*, **29**, 231–237.

Hulliger F. (1964) Crystal structure and electrical properties of some cobalt-group chalcogenides. *Nature*, **204**, 644–646.

Kanmera K. (1952) The Upper Carboniferous and the Lower Permian of the Hikawa Valley, Kumamoto Pref., Kyushu, Japan. *The Journal of Geological Society of Japan*, **58**, 17–32.

Leblanc M. (1991) Platinum-group elements and gold in ophiolitic complexes: distribution and fractionation from mantle to oceanic floor. Pp. 231–260 in: *Ophiolite Genesis and Evolution of the Oceanic Lithosphere* (T. Peters, A. Nicolas and R.G. Coleman, editors). Springer, Dordrecht, Netherlands.

Legendre O. and Augé T. (1986) Mineralogy of platinum-group mineral inclusions in chromitites from different ophiolite complexes. Pp. 361–372 in: *Metallogeny of Basic and Ultrabasic Rocks* (M.J. Gallagher, R.A. Ixer, C.R. Neary and H.M. Prichard, editors). Proceedings of the Conference Metallogeny of Basic and Ultrabasic Rocks, held in Edinburgh, Scotland, 9-12 April. The Institution of Mining and Metallurgy, London.

Leonard B.F., Desborough G.A. and Page N.J. (1969) Ore microscopy and chemical composition of some laurites. *American Mineralogist*, **54**, 1330–1346.

Levien L., Weidner D.J. and Prewitt C.T. (1979) Elasticity of diopside. *Physics and Chemistry of Minerals*, **4**, 105–113.

Lutz H.D., Müller B., Schmidt Th. and Stingl Th. (1990) Structure refinement of pyrite-type ruthenium disulfide, RuS_2, and ruthenium diselenide, $RuSe_2$. *Acta Crystallographica*, **C46**, 2003–2005.

Matsumoto A. (1928) Placer gold and platinum–group minerals from Hokkaido. *Journal of the Mining Institute of Japan*, **44**, 737–745.

Melcher F., Grum W., Simon G., Thalhammer T.V. and Stumpfl E.F. (1997) Petrogenesis of the ophiolitic giant chromite deposits of Kempirsai, Kazakhstan: a study of solid and fluid inclusions in chromite. *Journal of Petrology*, **38**, 1419–1458.

Mertie Jr., J.B. (1969) *Economic Geology Of The Platinum Metals*. U.S. Geological Survey Professional Paper, v. 630. USGS, Colorado, USA.

Momma K. and Izumi F. (2011) *VESTA* 3 for three-dimensional visualization of crystal, volumetric and morphology data. *Journal of Applied Crystallography*, **44**, 1272–1276.

Munson R.A. (1968) The synthesis of iridium disulfide and nickel diarsenide having the pyrite structure. *Inorganic Chemistry*, **7**, 389–390.

Nakagawa M. and Franco H.E.A. (1997) Placer Os-Ir-Ru alloys and sulfides; indicators of sulfur fugacity in an ophiolite? *The Canadian Mineralogist*, **35**, 1441–1452.

Nakagawa M. and Ohta E. (1993) Placer platinum–group minerals from ophiolite in Hokkaido. Pp. 133–141 in: *Professor Jiro ISHII Memorial Volume*. Niigata, Japan [in Japanese].

Nakagawa M., Ohta E. and Kurosawa K. (1991) Platinum-group minerals from the Mukawa serpentinite, southern Kamuikotan belt, Japan. *Mining Geology*, **41**, 329–335.

Nishio-Hamane D., Tanaka T. and Shinmachi T. (2019) Minakawaite and platinum–group minerals in the placer from the clinopyroxenite area in serpentinite mélange of Kurosegawa belt, Kumamoto Prefecture, Japan. *Journal of Mineralogical and Petrological Sciences*, **114**, 252–262.

Nowack E., Schwarzenbach D. and Hahn Th. (1991) Charge densities in CoS_2 and NiS_2 (pyrite structure). *Acta Crystallographica*, **B47**, 650–659.

Ohta E. and Nakagawa M. (1990) Placer PGE alloys from Fukuyama, Hobetsu, Hokkaido, Japan. *Bulletin of the Hobetsu Museum*, **6**, 15–23.

Osanai Y., Yoshimoto A., Nakano N., Adachi T., Kitano I., Yonemura K., Sasaki J., Tsuchiya N. and Ishizuka H. (2014) LA-ICP-MS zircon U-Pb geochronology of Paleozoic granitic rocks and related igneous rocks from the Kurosegawa tectonic belt in Kyushu, Southwest Japan. *Japanese Magazine of Mineralogical and Petrological Sciences*, **43**, 71–99.

Parthé E., Hohnke E. and Hulliger F. (1967) A new structure type with octahedron pairs for Rh_2S_3, Rh_2Se_3 and Ir_2S_3. *Acta Crystallographica*, **23**, 832–840.

Pauling L. (1940) *The Nature of the Chemical Bond*. 3rd edition. Cornell University Press, Ithaca, New York, USA, 518 pp.

Rettig S.J. and Trotter J. (1987) Refinement of the structure of orthorhombic sulfur, alpha-S_8. *Acta Crystallographica*, C43, 2260–2262.

Saito M., Miyazaki K. and Tsukamoto H. (2004) Clinopyroxenite in serpentinite mélange of the "Kurosegawa belt" in the Izumi–Tomochi area, Kumamoto Prefecture, central Kyushu. *Bulletin of the Geological Survey of Japan*, **55**, 171–179.

Saito M., Miyazaki K., Toshimitsu S. and Hoshizumi H. (2005) *Geology of the Tomochi district. Quadrangle Series, 1:50,000*. Geological Survey of Japan, AIST, Tsukuba, Japan.

Shannon R.D. (1976) Revised effective ionic radii and systematic studies of interatomic distances in halides and chalcogennides. *Acta Crystallographica*, **A32**, 751–767.

Shannon R.D., O'Keeffee M. and Navrotsky A. (1981) *Structure and Bonding in Crystals*. Academic Press, New York, 53–70 pp.

Sheldrick G.M. (2015) *SHELXT* – Integrated space-group and crystal-structure determination. *Acta Crystallographica Section*, **A71**, 3–8.

Snetsinger K.G. (1971) Erlichmanite (OsS_2), a new mineral. *American Mineralogist*, **56**, 1501–1506.

Stassen W.N. and Heyding R.D. (1968) Crystal structures of $RuSe_2$, $OsSe_2$, $PtAs_2$, and α-$NiAs_2$. *Canadian Journal of Chemistry*, **46**, 2159–2163.

Stingl Th., Müller B. and Lutz H.D. (1992) Crystal structure refinement of osmium(II) disulfide, OsS_2. *Zeitschrift für Kristallographie – Crystalline Materials*, **202**, 161–162.

Stockman H.W. and Hlava P.F. (1984) Platinum-group minerals in alpine chromitites from southwestern Oregon. *Economic Geology*, **79**, 491–508.

Sumino Y. (1979) The elastic constants of Mn_2SiO_4, Fe_2SiO_4 and Co_2SiO_4, and the elastic properties of olivine group minerals at high temperature. *Journal of Physics of the Earth*, **27**, 209–238.

Sumino Y., Nishizawa O., Goto T., Ohno I. and Ojima M. (1977) Temperature variation of elastic constants of single-crystal forsterite between–190° and 400°C. *Journal of Physics of the Earth*, **25**, 377–392.

Sutarno, Knop O. and Reid K.I.G. (1967) Chalcogenides of the transition elements. V. Crystal structures of the disulfides and ditellurides of ruthenium and osmium. *Canadian Journal of Chemistry*, **45**, 1391–1400.

Thomassen L. (1929) Über Kristallstrukturen einiger binärer Verbindungen der Platinmetalle II. *Zeitschrift für Physikalische Chemie*, **4B**, 277–287.

Tokuda M., Yoshiasa A., Mashimo T., Arima H., Hongu H., Tobase T., Nakatsuka A. and Sugiyama K. (2019) Crystal structure refinement of $MnTe_2$, $MnSe_2$, and MnS_2: cation-anion and anion–anion bonding distances in pyrite-type structures. *Zeitschrift für Kristallographie – Crystalline Materials*, **234**, 371–377.

Torres-Ruiz J., Garuti G., Gazzotti M., Gervilla F. and Hach-Ali P.F. (1996) Platinum-group minerals in chromitites from the ojen lherzolite massif (Serrania de Ronda, Betic Cordillera, Southern Spain). *Mineralogy and Petrology*, **56**, 25–50.

Tredoux M., Lindsay N.M., Davies G. and McDonald I. (1995) The fractionation of platinum-group elements in magmatic systems, with the suggestion of a novel causal mechanism. *South African Journal of Geology*, **98**, 157–167.

Unoki K., Yoshiasa A., Kitahara G., Nishiyama T., Tokuda M., Sugiyama K. and Nakatsuka A. (2021) Crystal structure refinements of stoichiometric Ni_3Se_2 and NiSe. *Acta Crystallographica*, **C77**, 169–175.

Weidner D.J., Wang H. and Ito J. (1978) Elasticity of orthoenstatite. *Physics of the Earth and Planetary Interiors*, **17**, 7–13.

Willis B.T.M. and Pryor A.W. (1975) *Thermal Vibrations in Crystallography*. Cambridge University Press, Cambridge, UK.

Wöhler F. (1866) Ueber Laurit, ein neues Mineral aus Borneo. *Journal für Praktische Chemie*, **98**, 226–228.

Wood, I.G., Knight, K.S., Price, G.D. and Stuart, J.A. (2002) Thermal expansion and atomic displacement parameters of cubic $KMgF_3$ perovskite determined by high-resolution neutron powdser diffraction. *Journal of Applied Crystallography*, **35**, 291–295.

Yoshiasa A., Nakatani T., Nakatsuka A., Okube M., Sugiyama K. and Mashimo T. (2016) High-temperature single-crystal X-ray diffraction study of tetragonal and cubic perovskite-type $PbTiO_3$ phases. *Acta Crystallographica Section*, **B72**, 381–388.

Yoshiasa A., Tokuda M., Kitahara G., Unoki K., Isobe H., Nakatsuka A. and Sugiyama K. (2021) Crystal synthesis and Debye temperature determination of $PdSb_2$: Usefulness of single crystal precise structure analysis. *Journal of Crystal Growth*, **574**, 126327.

https://doi.org/10.1180/mgm.2022.139 Published online by Cambridge University Press